Kinetic imaging of NPC1L1 and sterol trafficking between plasma membrane and recycling endosomes in hepatoma cells[s]

Nicole Hartwig Petersen,* Nils J. Færgeman,* Liqing Yu,[†] and Daniel Wüstner[1],*

Department of Biochemistry and Molecular Biology,* University of Southern Denmark, Campusvej 55, Odense M, DK-5230 Denmark; Department of Pathology,[†] Section on Lipid Sciences, Wake Forest University School of Medicine, Winston-Salem, NC 27157-1040

Abstract Niemann-Pick C1-like 1 (NPC1L1) is a recently identified protein that mediates intestinal cholesterol absorption and regulates biliary cholesterol excretion. The itineraries and kinetics of NPC1L1 trafficking remain uncertain. In this study, we have visualized movement of NPC1L1-enhanced green fluorescent protein (NPC1L1-EGFP) and cholesterol analogs in hepatoma cells. At steady state, about 42% of NPC1L1 resided in the transferrin (Tf)-positive, sterol-enriched endocytic recycling compartment (ERC), whereas time-lapse microscopy demonstrated NPC1L1 traffic between the plasma membrane and the ERC. Fluorescence recovery after photobleaching revealed rapid recovery (half-time ~2.5 min) of about 35% of NPC1L1 in the ERC, probably replenished from peripheral sorting endosomes. Acute cholesterol depletion blocked internalization of NPC1L1-EGFP and Tf and stimulated recycling of NPC1L1-EGFP from the ERC to the plasma membrane. NPC1L1-EGFP facilitated transport of fluorescent sterols from the plasma membrane to the ERC. Insulin induced translocation of vesicles containing NPC1L1 and fluorescent sterol from the ERC to the cell membrane. Upon polarization of hepatoma cells, NPC1L1 resided almost exclusively in the canalicular membrane, where the protein is highly mobile.[JLR] Our study demonstrates dynamic trafficking of NPC1L1 between the cell surface and intracellular compartments and suggests that this transport is involved in NPC1L1-mediated cellular sterol uptake.—Petersen, N. H., N. J. Færgeman, L. Yu, and D. Wüstner. **Kinetic imaging of NPC1L1 and sterol trafficking between plasma membrane and recycling endosomes in hepatoma cells.** *J. Lipid Res.* 2008. **49:** **2023–2037.**

Supplementary key words cholesterol • fluorescence microscopy • dehydroergosterol • cholestatrienol • kinetics • intestine • liver • absorption • bile • Niemann Pick C1-like 1

Niemann-Pick C1-like 1 (NPC1L1) was recently identified as a protein mediating intestinal cholesterol absorption (1). NPC1L1 is a target of the potent cholesterol absorption inhibitor ezetimibe, which has been widely used to lower plasma total cholesterol and LDL-cholesterol (2, 3). In the liver, NPC1L1 protein localizes at the canalicular membrane of hepatocytes (4, 5). It regulates biliary cholesterol excretion, probably by transporting cholesterol back into hepatocytes from canalicular bile (5). The molecular and cellular basis for NPC1L1-dependent cholesterol transport remains to be elucidated. Considerable disagreement exists regarding the subcellular localization and function of NPC1L1. Both intracellular and cell surface locations have been reported for NPC1L1 protein (1, 2, 4–9). Some studies suggest that NPC1L1 acts at the cell surface, mediating sterol entry into cells (1, 2, 4, 5, 9, 10). Others report that NPC1L1 resides mainly in intracellular compartments in some cultured nonpolarized cells, where NPC1L1 protein, like Niemann Pick C1 protein (NPC1), may mediate intracellular sterol transport (8, 11, 12). Recent data demonstrate that NPC1L1 tagged with enhanced green fluorescent protein (NPC1L1-EGFP) colocalizes with transferrin (Tf) in the perinuclear endocytic recycling compartment (ERC) of McArdle RH7777 rat hepatoma (McA) cells (4). In nonpolarized human hepatoma HepG2 cells, immunofluorescence revealed colocalization of NPC1L1 with rab5, a marker for sorting endosomes (10). Sorting endosomes are a population of early endosomes that iteratively deliver

recycling receptors, lipids, and other membrane proteins to the long-living ERC by pinching off small vesicles and tubules (13). The sorting endosomes are transient organelles that lose their fusion competence for incoming vesicles with a half-time of approximately 8 min, and eventually mature into late endosomes (14, 15). After endocytosis, fluorescent Tf is first transported to sorting endosomes with a half-time of about 2 min (15). After iron release, receptor-bound Tf is shuttled from sorting endosomes to the ERC, where the Tf accumulates, owing to its slow exit from this compartment and recycling back to the surface (13). Therefore, fluorescent Tf is often used as a marker for the ERC and for sorting endosomes in membrane trafficking studies. Transport of fluorescent Tf and lipids between sorting endosomes and the ERC is rapid [half time ($t_{1/2}$) $\sim$2 min] and bidirectional (16, 17). Previous work demonstrated that endocytosis and transport of Tf from sorting endosomes to the ERC, but not recycling of Tf from the ERC to the cell surface, depends on intact microtubules (18–20). Fluorescent Tf experiences several rounds of endocytosis and recycling before being eventually released from the receptor at the cell surface. In polarized (hepatic) cells, fluorescent Tf accumulates in a subapical recycling compartment that largely resembles the ERC of nonpolarized cells, with the additional function of sorting proteins and lipids between the apical and basolateral plasma membrane domains (21–24).

Interestingly, the subcellular localization of NPC1L1 was found to be responsive to cellular cholesterol availability, with cholesterol depletion induced by cyclodextrin causing the protein to accumulate in the plasma membrane (4, 25). It remains to be clarified whether this shift in steady-state distribution of NPC1L1 upon cholesterol depletion is caused by inhibition of endocytosis, by stimulation of recycling from intracellular pools, or by both processes operating in parallel. For fluorescent Tf, a marker for clathrin-dependent endocytosis, it is known that acute cholesterol depletion blocks Tf uptake without affecting recycling of internal Tf to the cell surface (26, 27). Previous work demonstrated that NPC1L1 mediates unidirectional cholesterol uptake into hepatoma cells in a time course of 30 min to 2 h, and this process was facilitated by increasing the amount of protein in the plasma membrane via cholesterol depletion (4, 11, 25). The amount of free cholesterol was doubled in McA cells expressing NPC1L1-EGFP, compared with control cells when cultured in cholesterol-containing medium (4). This suggests that the presence of NPC1L1 alone is sufficient to increase cellular cholesterol levels in hepatoma cells. Acute cholesterol depletion using the cholesterol chelator cyclodextrin was used previously to facilitate cellular uptake of unesterified cholesterol by NPC1L1 and to be able to monitor this process using radioactive cholesterol tracer (4, 25).

Here, we have performed a kinetic imaging study on transport of NPC1L1-EGFP in hepatoma cells. Focus was set on a detailed comparison of trafficking of NPC1L1 with that of fluorescent Tf under control and cholesterol depletion conditions. We also investigated transport of NPC1L1 in polarized human hepatoma HepG2 cells. The HepG2 cell line is able to form apical bile canaliculi (BC)-like structures resembling the canaliculi biliferi of the liver (28). This cell line is therefore often used to investigate polarized transport processes as they occur in hepatocytes (24, 29). Polarized HepG2 cells are also a suitable model system to investigate hepatocyte-specific lipid and sterol transport processes (22, 30–34). Finally, we used the intrinsically fluorescent close cholesterol analogs dehydroergosterol (DHE) and cholestatrienol (CTL) to determine whether NPC1L1 plays a role in sterol transport from the plasma membrane. Fluorescent sterols like DHE or CTL can be transferred quickly and efficiently to the plasma membrane from cyclodextrin donor complexes, allowing for kinetic sterol trafficking studies using pulse-chase protocols (35, 36). We show that NPC1L1 shuttles dynamically between the plasma membrane and the ERC, and we provide evidence for a function of NPC1L1 in vesicular sterol transport from the plasma membrane to the recycling endosomes in polarized and nonpolarized hepatoma cells.

EXPERIMENTAL PROCEDURES

Chemicals

Rhodamine-labeled dextran (Rh-dextran; 70 kDa), 1,1′-didodecyl-3,3,3′,3′-tetramethylindocarbocyanine perchlorate (DiIC12), Alexa-546, and Alexa-488 were purchased from Molecular Probes, Inc. CTL was obtained from Avanti Polar Lipids. Medium 1 contained 150 mM NaCl, 5 mM KCl, 1 mM CaCl$_2$, 1 mM MgCl$_2$, 5 mM glucose, and 20 mM HEPES (pH 7.4). Medium 2 was identical to medium 1 except that it contained no glucose but 5 mM sodium azide and 50 mM 2-deoxyglucose for energy depletion of cells (see below). Fetal calf serum (FCS) and DMEM were from GIBCO BRL (Life Technologies, Paisley, Scotland). All other chemicals were from Sigma Chemical (St. Louis, MO). Transferrin (Tf) was iron loaded as previously described (37). Succinimidyl ester of Alexa-546 was then conjugated to the iron-loaded Tf following the manufacturer's instructions.

Cell culture and transfection

HepG2 and McArdle RH7777 (McA) cells were grown in DMEM with 4.5 g/l glucose, supplemented with 10% heat-inactivated FCS and antibiotics. Mammalian hepatoma cells expressing plasmid of human NPC1L1 protein, with EGFP appended at its C terminus (NPC1L1-EGFP) and McA cells stably expressing NPC1L1-EGFP, have been reported previously (4). Cells were routinely passaged in plastic tissue culture dishes. NPC1L1-EGFP fusion protein was stably expressed in HepG2 cells after transfection of NPC1L1-EGFP-expressing plasmid (4) using the lipofectamine transfection system according to the manufacture's instructions (Invitrogen A/S, Taastrup, Denmark). For experiments, cells were plated onto glass coverslips coated with poly-D-lysine and used after 3 days, when the highest degree of polarization is reached in HepG2 cells (22).

Labeling of cells with fluorescent sterols, lipid probes, and endocytic markers

A stock solution of DHE or CTL (5 mM) was made in ethanol and stored under nitrogen. For labeling cells with DHE or CTL, analogs were loaded on methyl-β-cyclodextrin (MCD), giving a DHE- or CTL-MCD (DHE/MCD and CTL/MCD) solution, respectively, as described previously (35). McA or HepG2 cells were

routinely labeled with DHE/MCD or CTL/MCD for 1 min at 37°C. To visualize kinetically defined sorting endosomes, McA or HepG2 cells were labeled with 20 μg/ml Alexa546-tagged transferrin (Alexa546-Tf) for 1 min, washed, and chased for 5 min at 37°C. This short incubation ensured that internalized Tf was transported from the cell surface to sorting endosomes before being targeted to the perinuclear ERC. To stain the ERC and subapical recycling compartment, respectively, cells were labeled with 20 μg/ml Alexa546-Tf for 15 min, washed, and chased for 30 min at 37°C, or, alternatively, cells were labeled for 30 min, washed, and directly imaged after various chase times (chase-out experiment). For triple labeling experiments, cells were first labeled with fluorescent sterol, then washed and labeled for 5 min at 37°C with 20 μg/ml Alexa546-Tf, and then washed and chased for 30 min at 37°C. To determine colocalization of NPC1L1-EGFP with lysosomal markers, cells were prelabeled with 2.5 mg/ml Rh-dextran for 1 h at 37°C, washed, and imaged on a wide-field microscope as described below. In polarized hepatoma cells, this procedure is also suitable for visualizing the BC, because Rh-dextran is transported to the BC lumen after prolonged chase (30, 32, 38). DiI lipid labeling solution was prepared as described previously by binding analogs to fatty acid-free BSA (22, 39). McA cells expressing NPC1L1-EGFP were labeled with DiIC12 for 1 min at 37°C, washed, and either imaged directly or chased for another 30 min at 37°C in medium 1 before imaging on a wide-field microscope as described below.

Cholesterol depletion and insulin stimulation of McA cells

McA cells expressing NPC1L1-EGFP were labeled with 20 μg/ml Alexa546-Tf for 30 min at 37°C, washed, and incubated with medium 1 containing 2% MCD in the presence or absence of 20 μg/ml Alexa546-Tf for various times (0–80 min). At the end of the chase period, cells were washed with medium 1 and imaged as described below. For insulin stimulation, cells were first serum starved for 3 h to minimize PI3 kinase activation. Cells were incubated in medium 1 containing 200 nM insulatard, a long-acting insulin homolog, for 90 min at 37°C. Cells were steady-state labeled with DHE/MCD, as described above, and imaged on a wide-field fluorescence microscope.

Fluorescence microscopy and image analysis

Wide-field fluorescence microscopy and digital image acquisition were carried out using a Leica DMIRBE microscope with a 63×, 1.4 NA oil immersion objective (Leica Lasertechnik GmbH, Wetzlar, Germany) equipped with an Orca BT512 four-stage peltier and water cooled (−80°C) CCD camera (Hamamatsu Photonics, Inc., Hamamatsu City, Japan) and a Lambda SC smart shutter (Sutter Instrument Co., Novato, CA) driven by ImagePro Plus and ScopePro (Media Cybernetics, Inc., Silver Spring, MD). Optical components and excitation source were described previously (40). DHE and CTL were imaged in ultraviolet using a specially designed filter cube obtained from Chroma Technology Corp. with 335 nm (20 nm bandpass) excitation filter, 365 nm longpass dichromatic filter, and 405 nm (40 nm bandpass) emission filter. Rh-dextran, DiIC12, and Alexa546-Tf were imaged using a standard rhodamine filter set [535 nm, (50 nm bandpass) excitation filter, 565 nm longpass dichromatic filter, and 610 nm (75 nm bandpass) emission filter], whereas NPC1L1-EGFP was imaged using a standard fluorescein filter set [470 nm, (20 nm bandpass) excitation filter, 510 nm longpass dichromatic filter, and 537 nm (23 nm bandpass) emission filter]. To visualize the three-dimensional distribution of early endosomes in McA cells, we used either a confocal microscope (see below) or a wide-field fluorescence microscope in z-stacking modus with 0.3 μm step size and iterative

deconvolution to reassign out-of-focus light to the right image plane using the Huygens software (Scientific Volume Imaging, Hilversum, The Netherlands). Confocal microscopy was performed using a laser scanning inverted fluorescence microscope (Zeiss LSM 510 META; Zeiss, Jena, Germany) equipped with a 63× 1.4 NA plan Apochromat water immersion objective and a 37°C temperature control (Zeiss). Cells labeled with Alexa546-Tf were excited with a 1.0 milliwatt helium/neon laser emitting at 543 nm, and a 560 nm longpass filter was used for collecting emissions. EGFP fluorescence was collected with a 505–530 bandpass filter after excitation of NPC1L1-EGFP with a 25 milliwatt argon laser emitting at 488 nm. The two channels were scanned sequentially in a line-by-line mode, having only one laser line and one detector channel on at each time. Time-lapse sequences were recorded by increasing scan speeds on a temperature-controlled stage maintained at 35 ± 1°C. The microscope was located on a nitrogen-floated table to prevent vibrations and focus drift.

Fluorescence recovery after photobleaching

Regions of interest (ROIs) were defined according to the geometry of the ERC in McA cells or the apical BC in HepG2 cells, respectively. Fluorescence of NPC1L1-EGFP was selectively bleached in the ROI by continuous illumination with the argon laser at full power for 30 s. Fluorescence recovery into the ROI was monitored at reduced laser power over time using the time-lapse function of the Zeiss LSM510 Meta confocal system.

Image and data analysis

Image analysis for fluorescence microscopy was carried out using the software packages ImagePro Plus (Media Cybernetics, Inc., Silver Spring, MD) or ImageJ (developed at the U.S. National Institutes of Health and available on the Internet at http://rsb. info.nih.gov/ij). Determination and subtraction of crossover of fluorescence between the channels was performed as described (16, 39). For calculation of fluorescence intensity of fluorescent sterol in the ERC, each image of the time series was first corrected for background intensity (17). Fluorescence of DHE or CTL in the ERC was measured after highlighting this compartment from images (image segmentation) by two methods: i) after manually outlining the ERC based on the geometry of this compartment using the free hand tool in ImageJ; ii) by creating a binary mask for the ERC as defined by fluorescence of Alexa546-Tf using one threshold for all images. This mask was applied to the DHE image. Both methods gave identical results. Quantification of the steady-state distribution of NPC1L1-EGFP was performed on cells pulse-labeled with DiIC12 to highlight the plasma membrane. The cells were outlined from the DiI image, or occasionally (after histogram stretching to reveal plasma membrane staining of NPC1L1-EGFP), from the image of NPC1L1-EGFP itself. An ROI was defined for the cell outline and applied to the background-corrected but not contrast-processed image of NPC1L1-EGFP. Protein in the ERC was measured from a second ROI of the background-corrected image of NPC1L1-EGFP. Fluorescence of NPC1L1-EGFP in the ERC and plasma membrane was quantified from images prior to and after addition of MCD as described previously (35). The fluorescence ratio in ERC and total cell-associated intensity was calculated for NPC1L1-EGFP and Alexa546-Tf using Sigma Plot 6.0 (SPSS, Inc.). All quantifications of cellular intensity of fluorescent sterol or NPC1L1 from microscopy experiments included five to fifteen fields of cells with at least two measurements per field. The half-time of protein redistribution was fitted to a single exponential decay function of the form $y = A \cdot e^{-k \cdot t} + y_0$ using the same software. Fluorescence recovery to a given time

point was calculated after background subtraction using the following equation:

$$Fx_{recovery} = \frac{\dfrac{F_x - F_0}{F_{max} - F_0}}{Fx_{total}} \qquad (Eq.\ 1)$$

where F_x is fluorescence intensity to time point x, F_0 is fluorescence intensity right after bleaching, F_{max} is fluorescence intensity in the given ROI before bleaching, and F_{total} is the total cell-associated NPC1L1-EGFP fluorescence to the given time point. Normalization to total cell-associated GFP fluorescence was necessary to account for fluorescence loss due to photobleaching of protein during the experiment.

The following kinetic model was used for analysis of fluorescence recovery after photobleaching (FRAP) data (see Results section):

$$c_1 \xrightleftharpoons[k_1, k_{-1}]{} c_2 \qquad (Eq.\ 2)$$

where c_2 represents the ERC and c_1 an unknown compartment from which the fluorescence of NPC1L1-EGFP recovering in the ERC originates. The forward rate constant toward the ERC is k_1, whereas the rate constant describing transport back from the ERC (c_2) to the source compartment is k_{-1}. The recovery curve was fitted to the following model equation, which is a solution of the linear differential equation system describing the kinetic scheme in equation 2 (41):

$$c_2(t) = \frac{k_{-1}}{k_1 + k_{-1}} \cdot (1 - \exp(-(k_1 + k_{-1}) \cdot t)) \qquad (Eq.\ 3)$$

This model (equation 3) was fitted to the fluorescence recovery curve using a nonlinear regression based on the Levenberg-Marquardt algorithm implemented in Sigma Plot 6.0.

RESULTS

Dynamic association of NPC1L1 with the ERC in nonpolarized McA cells

Previous results demonstrated that NPC1L1-EGFP localizes to the recycling endosome, ERC, in McA cells, but information about the dynamics of NPC1L1 protein is missing (4). As shown in **Fig. 1A**, NPC1L1-EGFP localized at steady state almost exclusively to the perinuclear ERC that was also stained with Alexa546-Tf. In this compartment, NPC1L1-EGFP also colocalized with the lipid-mimicking probe DiIC12 after 30 min chase at 37°C, a known marker
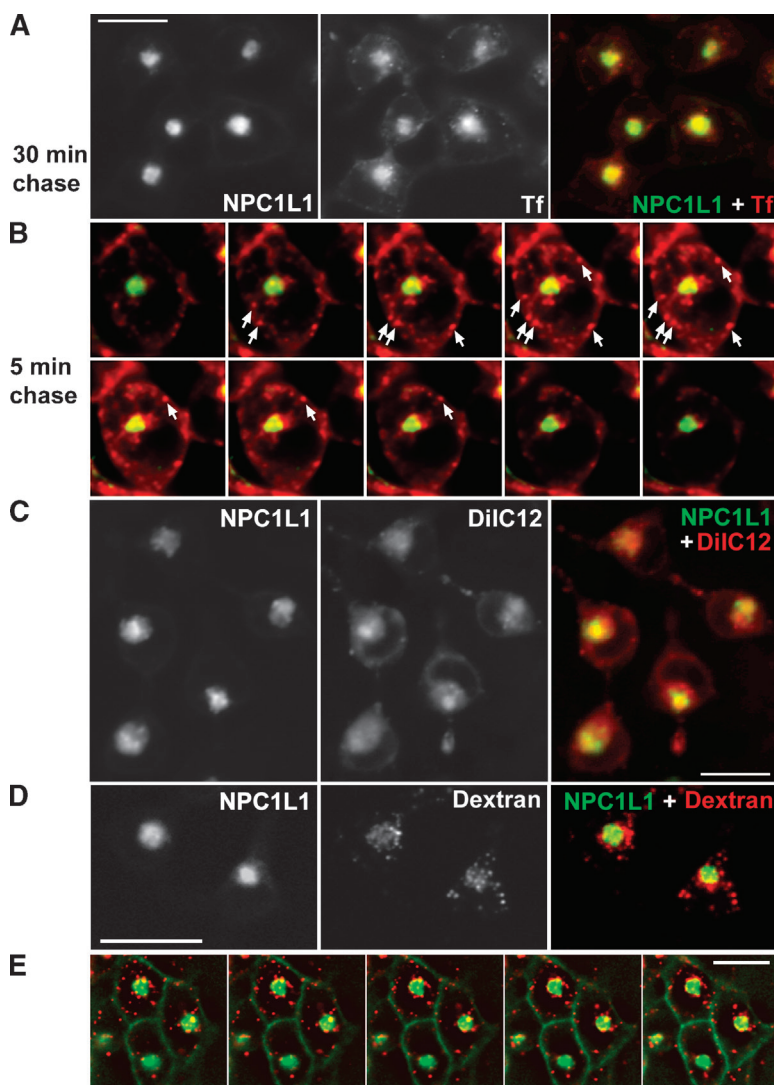

Fig. 1. Intracellular localization of Niemann Pick C1-like 1 enhanced green fluorescent protein (NPC1L1-EGFP) in nonpolarized McA cells. A, B: NPC1L1-EGFP-expressing McA cells were incubated with 20 μg/ml Alexa546-transferrin (Alexa546-Tf) for either 1 min (B) or for 15 min (A) at 37°C, washed, and chased for either 4 min to label early sorting endosomes (B, arrows) or for or 30 min to label the endocytic recycling compartment (ERC), respectively (A). A: Single plane wide-field image. B: Planes of a wide-field z-stack acquired with 0.3 μm step distance after deconvolution using the Huygens software (Scientific Volume Imaging; Hilversum, The Netherlands). Red, Alexa546-Tf; green, NPC1L1-EGFP. C: McA cells expressing NPC1L1-EGFP were pulse-labeled with the lipid probe DiIC12, washed, and chased for 30 min at 37°C. Red, DiIC12; green, NPC1L1-EGFP. D, E: McA cells were preincubated with rhodamine dextran (Dextran) for 1 h at 37°C, washed, and imaged on a wide-field microscope in z-stack modus. D: Sum projection of six planes. E: Individual planes being acquired 0.3 μm apart, with rhodamine dextran in red and NPC1L1-EGFP in green. Bar, 20 μm.

for the endocytic recycling pathway (Fig. 1C). A short pulse of 1 min with Alexa546-Tf, followed by a chase of 4 min at 37°C, was used to label peripheral sorting endosomes with fluorescent Tf (Fig. 1B). These kinetically defined sorting endosomes did not contain detectable amounts of NPC1L1-EGFP (arrows, Fig. 1B; see Experimental Procedures). We did find colocalization of both proteins in peripheral endosomes at later time points (see below, Fig. 4). NPC1L1-EGFP was not targeted to late endosomes or lysosomes prelabeled with Rh-dextran in McA cells (Fig. 1D, E). In a time-lapse experiment, we observed trafficking of NPC1L1-EGFP-containing vesicles between the ERC and the plasma membrane (**Fig. 2**). Endocytic vesicles containing NPC1L1-EGFP moved from the plasma membrane toward the ERC in a time course of 5 min (red circles, Fig. 2A, B). We found also vesicles with NPC1L1-EGFP originating at the ERC that move to the cell surface and probably fuse with it (green circles, Fig. 2A, C). Dual-color time-lapse studies revealed
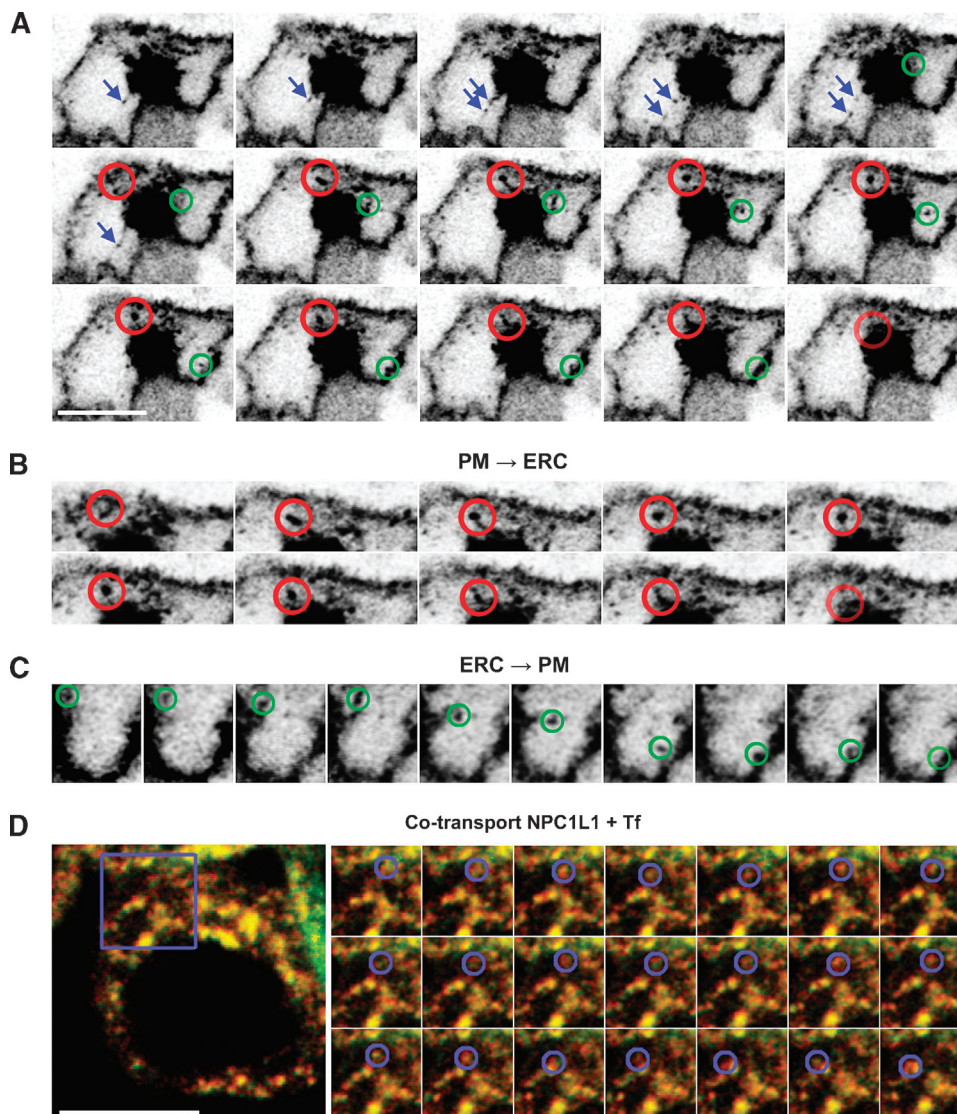

Fig. 2. Time-lapse imaging of NPC1L1-EGFP in McA cells. A–C: McA cells expressing NPC1L1-EGFP were placed on the temperature-controlled stage of a confocal microscope maintained at $35 \pm 1°C$, and images were acquired with high scan speed every 30 sec and a pinhole of three Airy disks with an argon laser at low power to reduce photobleaching. Endocytic vesicle trafficking between the endocytic recycling compartment (ERC) region (large central spot in the inverted images) and the plasma membrane (PM) was found at preferred sites (blue arrows, first row in A). A vesicle formed at the plasma membrane and moved toward the ERC pool in a time course of 5 min (red circle in A, middle and lower row, and B). In the same time course a vesicle containing NPC1L1-EGFP moved from the ERC pool to the cell surface, where it eventually fused with the plasma membrane (green circle in A, middle and lower row and panel C). D: McA cells were steady-state labeled with Alexa546-Tf as described in the legend to Fig. 1 and imaged by two-color confocal time-lapse microscopy with a time step of 10 s. Double-labeled vesicles moved in the ERC region over a period of about 4 min (zoomed box in D). Bar, 10 μm.

Dynamic imaging of NPC1L1 in hepatocytes 2027

that vesicles moving in the immediate ERC region had NPC1L1-EGFP as well as Alexa546-Tf (Fig. 2D).The time-lapse data clearly establish bidirectional trafficking of NPC1L1 between the plasma membrane and the ERC.

A FRAP experiment on the ERC pool of NPC1L1-EGFP on a confocal laser-scanning microscope demonstrated that approximately 35% of the fluorescence of NPC1L1-EGFP recovers rapidly in the ERC, whereas the majority (65% of initial) did not recover over the time-course of the experiment (**Fig. 3A, B**). To determine the transport rates of the dynamic, rapidly recovering pool, we used a simple kinetic model described in Experimental Procedures (equations 2 and 3). A nonlinear regression of the FRAP data to this model gave the rate constants $k_1 = 0.399$ min^{-1} and $k_{-1} = 0.195$ min^{-1} describing transport to and from the ERC, respectively (see equations 2 and 3). These rates correspond to a half-time of $t_{1/2} = 1.74$ min and $t_{1/2} = 3.3$ min,

respectively. Such rapid kinetics is too fast for known endocytic trafficking from the plasma membrane to the ERC in mammalian cells, making it unlikely that fluorescence of NPC1L1-EGFP recovering in the bleached area originates from the cell surface (15, 42). Note that the recovery curve could be fitted equally well with a single exponential function of the form $c(t) = A \cdot (1 - e^{-k \cdot t})$, which models an unidirectional transport process. This gave a rate constant $k = 0.593$ min^{-1} corresponding to a half-time of $t_{1/2} = 1.16$ min. On the basis of both models, we conclude that fluorescence of NPC1L1-EGFP recovering in the ERC does not originate from the plasma membrane, but from an adjacent endosomal compartment, probably from sorting endosomes (see Discussion).

To determine the steady-state distribution of NPC1L1, we measured the total and ERC-associated NPC1L1-EGFP fluorescence intensity in McA cells pulse-labeled with a red
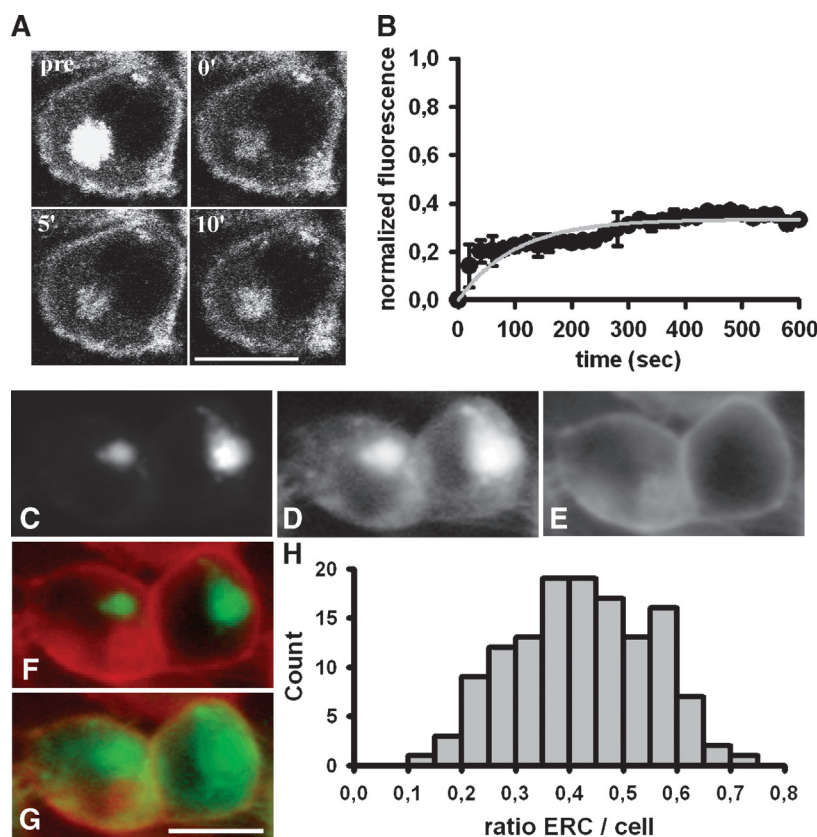

Fig. 3. Fluorescence recovery after photobleaching analysis and quantification of steady-state distribution of NPC1L1. A, B: Fluorescence recovery after photobleaching (FRAP) experiment on a confocal microscope. Fluorescence of NPC1L1-EGFP was bleached in the ERC by an intense pulse of the argon laser to about 20% of the prebleach intensity, followed by recording of fluorescence recovery with reduced laser power over a total time of 10 min. B: Quantification of ERC-associated fluorescence of NPC1L1-EGFP plotted as mean ± SE of seven independent experiments (black symbols). Longer observation to up to 30 min did not result in recovery higher than 35% of the prebleach intensity. Gray line, fit to the model given in equation 3. Bar, 10 μm. C–H: Quantification of the ERC pool size of NPC1L1-EGFP at steady state. McA cells expressing NPC1L1-EGFP were pulse-labeled with DiIC12 to visualize the plasma membrane, and ERC-associated NPC1L1 was quantified as described in Experimental Procedures. C: NPC1L1 raw data. D: NPC1L1 contrast-stretched to reveal surface staining of the protein. E: DiIC12. F, G: Color overlay, with NPC1L1 in green and DiIC12 in red for raw data image (F, compare C) and contrast-stretched image (G, compare D). H: Histogram of steady-state ratio of ERC to total cell-associated fluorescence of NPC1L1-EGFP (n = 134). Bar, 20 μm.

fluorescent DiIC12 lipid. This probe stains the plasma membrane and allows for ease in determination of cell outlines (see Experimental Procedures). The quantification shows that 42.44 ± 1.1% of total cell-associated NPC1L1-EGFP resides in the ERC at steady state (Fig. 3C–H). The remaining NPC1L1 should localize to the plasma membrane and, to a low extent, to peripheral sorting endosomes. To sustain this conclusion, we compared the steady-state distribution of NPC1L1-EGFP with that of Alexa546-Tf (**Fig. 4A**). From the fluorescence ratio of Alexa546-Tf to NPC1L1-EGFP in endosomes, we found that NPC1L1 becomes more enriched in the perinuclear ERC compared with fluorescent Tf, whereas the latter is more localized to peripheral sorting endosomes (compare Figs. 4A, 1B). In line with previous results (see above and Refs. 18–20), we found that disruption of microtubules with nocodazole increased the surface fraction of Alexa546-Tf and raised the amount of this fluorescent probe in peripheral sorting endosomes (Fig. 4B). Microtubule disruption had a qualitatively similar but much less pronounced effect on the steady-state distribution of NPC1L1-EGFP (Fig. 4C–G). Some NPC1L1-EGFP redistributed to the cell surface and was found in peripheral sorting endosomes, partially overlapping with Alexa546-Tf (arrows, Fig. 4E–G). This experiment suggests that internalization of both proteins and their transport from sorting endosomes to the ERC requires intact microtubules.

Cholesterol depletion reveals dynamic exchange of NPC1L1 between plasma membrane and ERC

To get further insight into the dynamics of NPC1L1's transport between plasma membrane and endosomes, we depleted cholesterol from cells using MCD (4). This treatment induced a shift in the steady-state distribution of NPC1L1-EGFP from the ERC to the plasma membrane, as previously described and confirmed here (**Fig. 5A, B**) (4). It remains to be clarified how this altered distribution of NPC1L1 is generated (see above). To answer this question, McA cells expressing NPC1L1-EGFP were steady-state labeled with Alexa546-Tf to load the ERC with fluorescent Tf and chased for 1 h either in the absence or in the presence of MCD (Fig. 5C–E). Under both conditions, Alexa546-Tf is efficiently chased out due to recycling of the ligand and release from the cell surface (middle panel in Fig. 5D, E). In cells treated with MCD, but not in control cells, NPC1L1-EGFP and most of the little remaining Alexa546-Tf were found in the plasma membrane. When Alexa546-Tf was present during the chase in medium 1 containing MCD to prevent chase-out of this fluorescent marker (16, 43), we observed a decrease of NPC1L1-EGFP
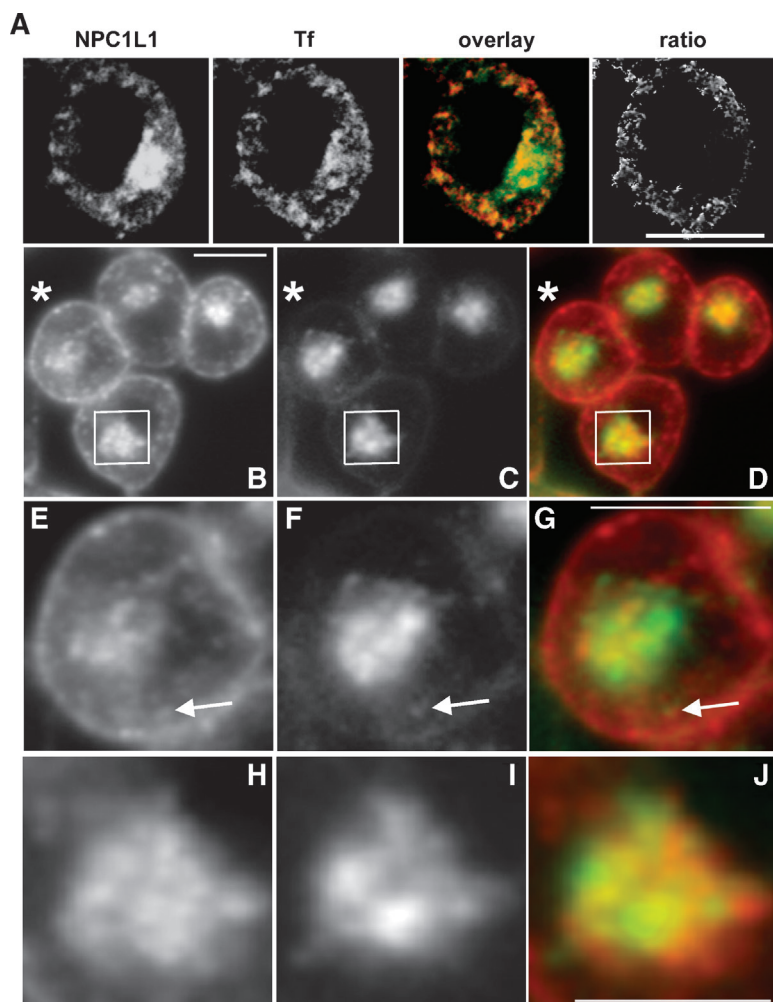

Fig. 4. Comparison of NPC1L1-EGFP and Alexa546-Tf in control and nocodazole-treated cells. McA cells expressing NPC1L1-EGFP were incubated in the absence (A) or presence (B–J) of 33 μM nocodazole for 30 min at 37°C, steady-state labeled with 20 μg/ml Alexa546-Tf as described in the legend to Fig. 1, washed, and imaged on a confocal (A) or wide-field microscope (B–J). A: Sum projection of a 3D stack of 10 confocal planes. Color overlay (NPC1L1, green; Tf, red) and ratio image calculated for Alexa546-Tf and NPC1L1-EGFP reveal more NPC1L1 in the ERC than in peripheral sorting endosomes, compared with Alexa546-Tf. B–J: Cells preincubated with nocodazole to disrupt microtubules show strongly increased Alexa546-Tf (B) and slightly increased NPC1L1-EGFP (C) at the cell surface and in peripheral endosomes. E–G: Zoom of the cell indicated by a star in (B–D) show colocalization of both proteins in peripheral punctate vesicles, probably sorting endosomes (arrows). H–J: Zoom of the ERC region outlined by a box in B–D. D, G, J, and third panel of A: Alexa546-Tf in red and NPC1L1-EGFP in green. Colocalization appears yellow to orange. Bar, 10 μm (A–G), or 5 μm (H–J).
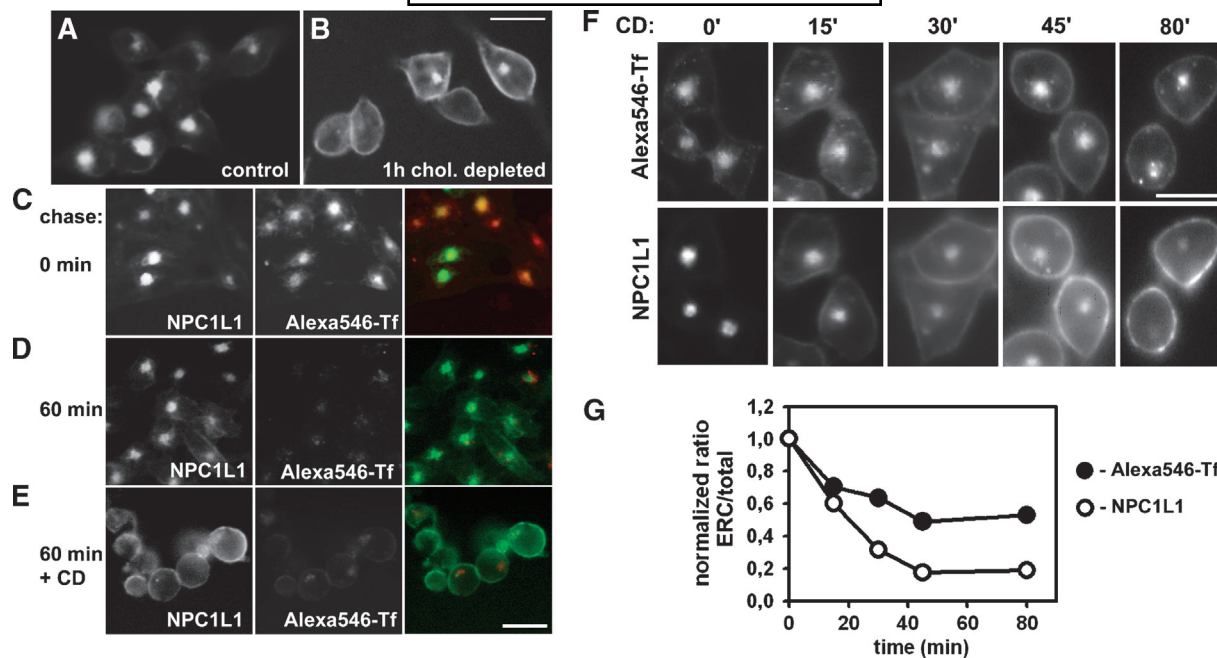
Fig. 5. Cholesterol depletion blocks endocytosis of NPC1L1 in McA cells. A, B: NPC1L1-EGFP-expressing McA cells were either left untreated (A) or incubated with methyl-β-cyclodextrin (MCD) in medium 1 for 1 h at 37°C and imaged (B). C–E: Cells were steady-state labeled with 20 µg/ml Alexa546-Tf in medium 1 for 30 min, washed, and chased for 0 min (C) or 1 h in the absence (D) or presence (E) of MCD at 37°C. F: Kinetics of redistribution of NPC1L1-EGFP and Alexa546-Tf in response to cholesterol depletion. Cells were labeled with Alexa546-Tf as described above, washed, and chased in the presence of MCD for 0, 15, 30, 45, and 80 min in medium 1 containing also 20 µg/ml Alexa546-Tf. Bar, 20 µm. G: Quantification of ERC-associated fluorescence as function of incubation time in the presence of MCD expressed as fraction of total cellular intensity of NPC1L1-EGFP (open symbols) and Alexa546-Tf (closed symbols). Data are expressed as mean ± SE from two different experiments with at least 10 measurements for each time point (error bars, smaller than symbol), and was normalized to the 0 min value from at least 10 fields.

and Alexa546-Tf in the ERC paralleled by an increased fraction of both proteins in the plasma membrane (Fig. 5F). Note that the decrease of fluorescence in the ERC as observed for Alexa546-Tf monitors inhibition of endocytosis by MCD, because previous experiments showed that recycling of Tf is unaffected by MCD treatment (26). We independently verified previous results showing that endocytosis of Alexa546-Tf was almost completely blocked in cells first depleted of cholesterol (26). Quantification of the fluorescence ratio in the ERC to total cell-associated fluorescence of NPC1L1-EGFP (Fig. 5G, open symbols) and Alexa546-Tf (Fig. 5G, filled symbols) allows us to compare the extent and kinetics of cholesterol depletion-induced redistribution of both proteins. The half-time of this shift in protein location from the ERC to the cell surface was comparable for both proteins (i.e., $t_{1/2} = 14.1$ min for NPC1L1-EGFP vs. $t_{1/2} = 12.2$ min for Alexa546-Tf, respectively). The extent of the redistribution measured as the plateau value of the fluorescence ratio (ERC/total) was larger for NPC1L1-EGFP than for fluorescent Tf (this is reflected by a residual of $y_0 = 0.6$ for Alexa546-Tf and $y_0 = 0.17$ for NPC1L1-EGFP, respectively; see Experimental Procedures for fitting details). Thus, proportionally more NPC1L1-EGFP than Alexa546-Tf redistributes from the ERC to the cell surface in response to MCD treatment. Note that inhibition of cholesterol synthesis using the statin mevalonin similarly increased the fraction of NPC1L1 in the plasma membrane (not shown).

Insulin stimulates translocation of NPC1L1 and sterol to the plasma membrane

We aimed to clarify whether the dynamic redistribution of NPC1L1 to the cell surface can be induced by stimuli other than cholesterol depletion. NPC1L1-EGFP colocalized strongly with the fluorescent sterol DHE in the ERC of McA cells (**Fig. 6A–C**). Insulin stimulation increased the fraction of NPC1L1-EGFP and DHE in the plasma membrane and reduced the ERC pool of protein and sterol (Fig. 6D–F). The amount of NPC1L1 and DHE in the ERC was lowered by 40% and 20%, respectively, upon insulin stimulation, as determined by image analysis tools described above and in Experimental Procedures. Vesicles containing NPC1L1-EGFP and DHE were found adjacent to the plasma membrane in insulin-stimulated but not in unstimulated cells (Fig. 6G–J). Note that insulin stimulation did not induce a higher DHE staining when pulse-labeling cells with DHE/MCD solution (not shown). Thus, increased amounts of sterol in the plasma membrane upon insulin stimulation are not caused by more-efficient labeling of cells with DHE but by increased sterol trafficking from intracellular pools.

NPC1L1 enhances sterol transport from the plasma membrane to the ERC

The results presented above prompted us to investigate whether NPC1L1 functions in sterol transport from the plasma membrane to intracellular compartments. We per-
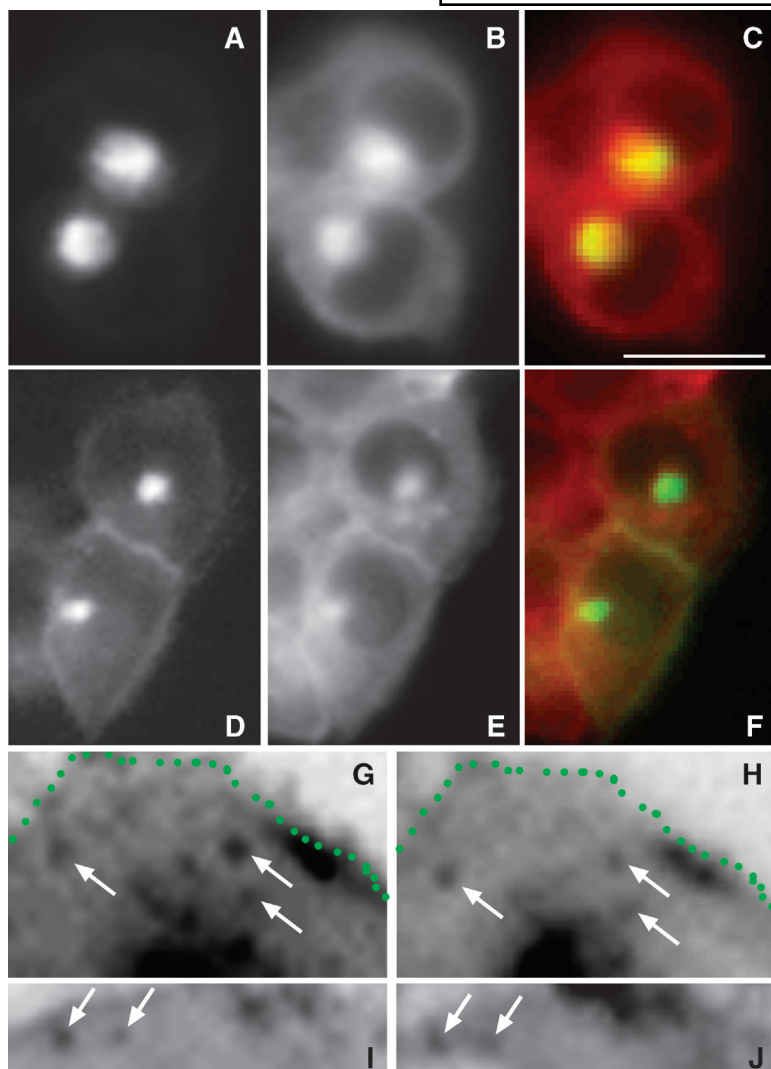
Fig. 6. Insulin stimulation shifts NPC1L1 to the cell surface of McA cells. McA cells expressing NPC1L1-EGFP were either left untreated (A–C) or serum starved for 3 h to minimize activity of PI3 kinases, followed by incubation with 200 nM of the insulin analog insulatard for 90 min at 37°C in medium 1 (D–F). Cells were washed, pulse labeled with dehydroergosterol (DHE), and chased for 30 min at 37°C in medium 1 containing insulatard. A, D: NPC1L1-EGFP. B, E: DHE. C, F: Color overlay with NPC1L1-EGFP in green and DHE in red. G–I: Double-labeled vesicles containing NPC1L1-EGFP (G, I) and DHE (H, J) were found in proximity to the plasma membrane (green dotted line in G, H) in response to insulatard treatment. G–J: Images were inverted for better visualization. Bar, 20 μm.

formed pulse-chase studies using the cholesterol-mimicking fluorescent sterols DHE and CTL. In both control and NPC1L1-expressing McA cells, we observed transport of DHE to the perinuclear ERC, visualized by coincubation with Alexa546-Tf (**Fig. 7A–H**). The same result was found for the other fluorescent sterol, CTL (not shown). Accumulation of DHE in the ERC over time, however, was more pronounced in McA cells having NPC1L1-EGFP compared with McA cells expressing just EGFP. Moreover, at long chase times, over 60 min at 37°C, DHE colocalized with NPC1L1-EGFP additionally in tubules and vesicles that emanated from the ERC region and lacked Alexa546-Tf, (Fig. 7A′-H′, I–K). Sterol and NPC1L1-EGFP accumulated in the most central part of the ERC, whereas fluorescent Tf appeared slightly more scattered (Fig. 7I–K). We quantified the ERC-associated fluorescence of DHE based on the geometry of the ERC as seen in the corresponding image of Alexa546-Tf (Fig. 7L, and Experimental Procedures). This analysis revealed that the time course of transport of fluorescent sterol from the plasma membrane to the ERC is very similar for control and NPC1L1-expressing McA cells in the first 30 min of incubation (Fig. 7M).

Whereas in control cells, the steady state was reached after a 30 min chase, in McA cells expressing NPC1L1-EGFP, the DHE continued to accumulate in the ERC over a time course of 2 h (Fig. 7M). In control cells, sterol transport to the ERC can be described with a single exponential function of the form $y(t) = A \cdot (1 - e^{-k \cdot t})$, giving an amplitude of 1.2 and a half-time of $t_{1/2} = 10.9$ min (Fig. 7M; black symbols, data; black line, fit). In contrast, in NPC1L1-expressing McA cells, transport of DHE to the ERC followed a bi-exponential process fitted with a double-exponential function of the form $y(t) = A \cdot (1 - \exp(-k_1 \cdot t)) + B \cdot (1 - \exp(-k_2 \cdot t))$ (Fig. 7M; gray symbols, data; gray line, fit). This regression gave a first phase having an amplitude of $A = 0.94$ and a half-time closely resembling that in control cells ($t_{1/2} = 8.0$ min) and a second slower phase (amplitude of $B = 1.45$, and half-time $t_{1/2} = 83.5$ min). Note that total cell-associated DHE was the same in control and NPC1L1-expressing cells. Thus, expression of NPC1L1-EGFP does not enhance sterol uptake during the short labeling pulse with DHE/MCD but increases intracellular sterol targeting from the plasma membrane to the ERC. To get insight into the mechanism of intracellular sterol
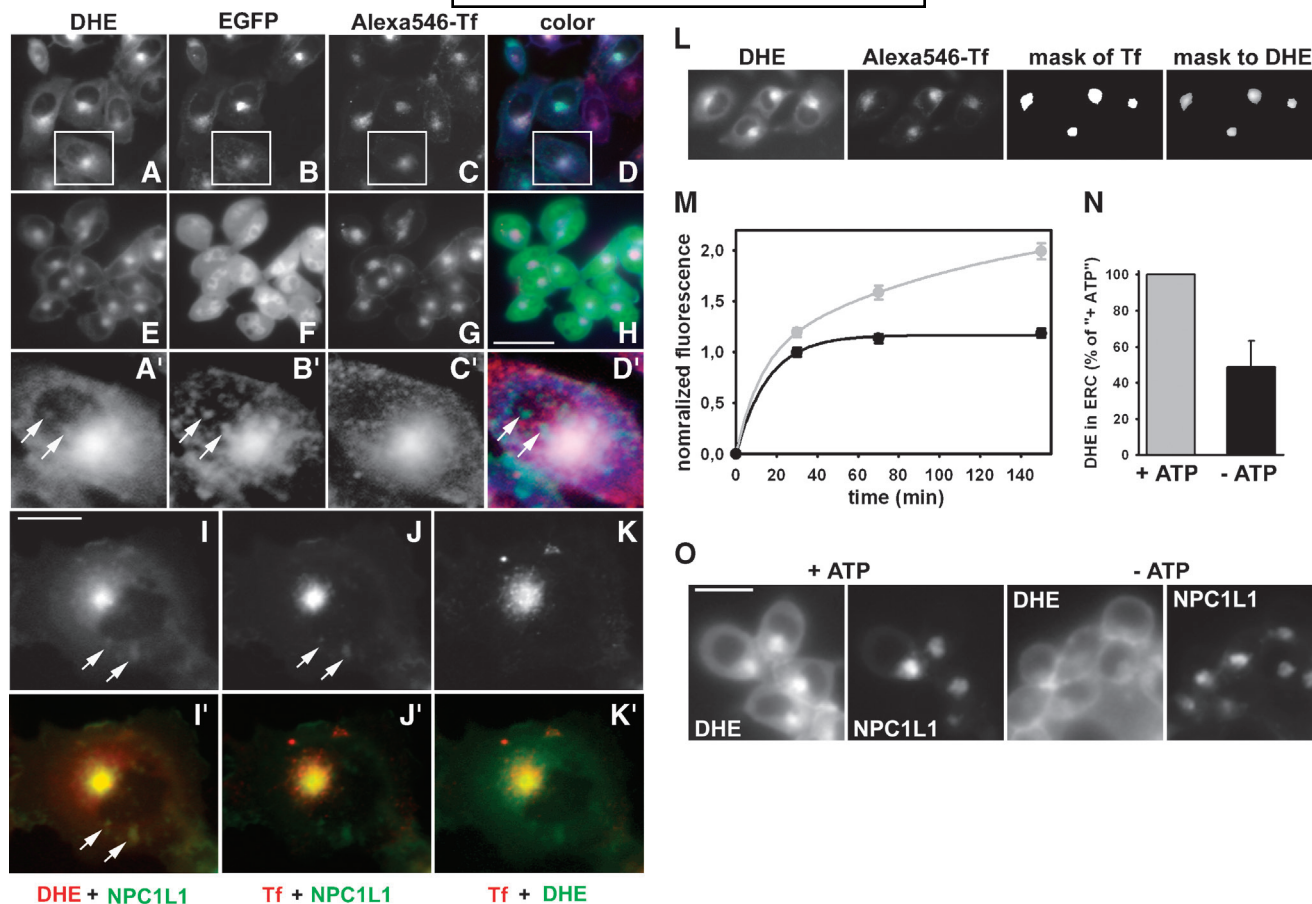
Fig. 7. NPC1L1 mediates intracellular accumulation of DHE in the ERC. McA cells expressing NPC1L1-EGFP (A–D′, I–K′) or expressing only EGFP (E–H) were pulse labeled with DHE/MCD for 2 min, washed, labeled with Alexa546-Tf for 15 min, and chased for 70 min at 37°C in medium 1. DHE (A, E, A′, I) colocalized with NPC1L1-EGFP (B, B′, J) and Alexa546-Tf (C, G, C′, K) in the perinuclear ERC, whereas expression of the EGFP vector resulted in diffuse cytoplasmic fluorescence (F). D, H, D′: triple-color overlay showing DHE in blue, EGFP in green, and Alexa546-Tf in red. A′–D′: Zoomed region of the outlined box in A–D showing vesicles containing DHE and NPC1L1-EGFP but not Alexa546-Tf. I′–K′: Double-color overlay with color coding as indicated in the legend below the panels. Arrows in I, I′, J point to vesicles containing DHE and NPC1L1-EGFP but not Alexa546-Tf. L: Image analysis protocol for quantification of DHE in the ERC of McA cells. A binary mask was generated from the perinuclear ERC as defined by fluorescence of Alexa546-Tf using one threshold for all images. This mask was applied to the DHE image. M: ERC-associated fluorescence of DHE normalized to total cellular intensity of the sterol in McA cells expressing just the EGFP vector (black symbols) or NPC1L1-EGFP (gray symbols). Data represent mean ± SE of two experiments with at least 10 measurements per time point. Black and gray lines show nonlinear regression of the data to a single or double exponential function for McA cells expressing only EGFP vector or NPC1L1-EGFP, respectively. N, O: McA cells expressing NPC1L1-EGFP were incubated in medium 1 (+ ATP) or in ATP depletion medium, medium 2 (− ATP), washed, and steady-state labeled with DHE as described in Experimental Procedures. N: Quantification of ERC-associated DHE in ATP-depleted cells (black bar) as percentage of control cells (gray bar) (mean ± SE of 15 measurements). Bar, 20 μm.

trafficking, we tested the ATP dependence of sterol transport to the ERC in McA cells (Fig. 7N, O). ATP depletion to levels that completely block endocytosis of Alexa546-Tf strongly reduced the fluorescence of DHE in the ERC region in control and NPC1L1-expressing McA cells. Quantification of ERC-associated fluorescence of DHE in cells with and without ATP depletion showed that endocytosis contributes by 48% to total sterol uptake in McA cells expressing NPC1L1-EGFP (Fig. 7N, O) and to a similar extent in McA cells expressing just EGFP (not shown). We conclude that NPC1L1 enhances sterol enrichment in the ERC, probably by enhancing vesicular transport of DHE from the plasma membrane to this endosomal compartment in hepatoma cells.

Distribution of NPC1L1-EGFP in polarized hepatoma cells

Hepatocytes are polarized epithelial cells underlying vectorial transport between the basolateral and apical plasma membrane domains. To put our results in a physiologically relevant setting, we also investigated the distribution of NPC1L1 and sterols in polarized hepatocyte-like cells. HepG2 hepatoma cells expressing NPC1L1-EGFP show a dramatic shift in the steady-state distribution of the protein upon cell polarization (**Fig. 8A–D**). In nonpolarized HepG2 cells, NPC1L1-EGFP resides in intracellular vesicles and, to a higher extent than in McA cells, in the plasma membrane (Fig. 8C, D). In polarized HepG2 cells, however, the majority of the protein is targeted to the apical BC, with low EGFP fluorescence detectable in the basolateral
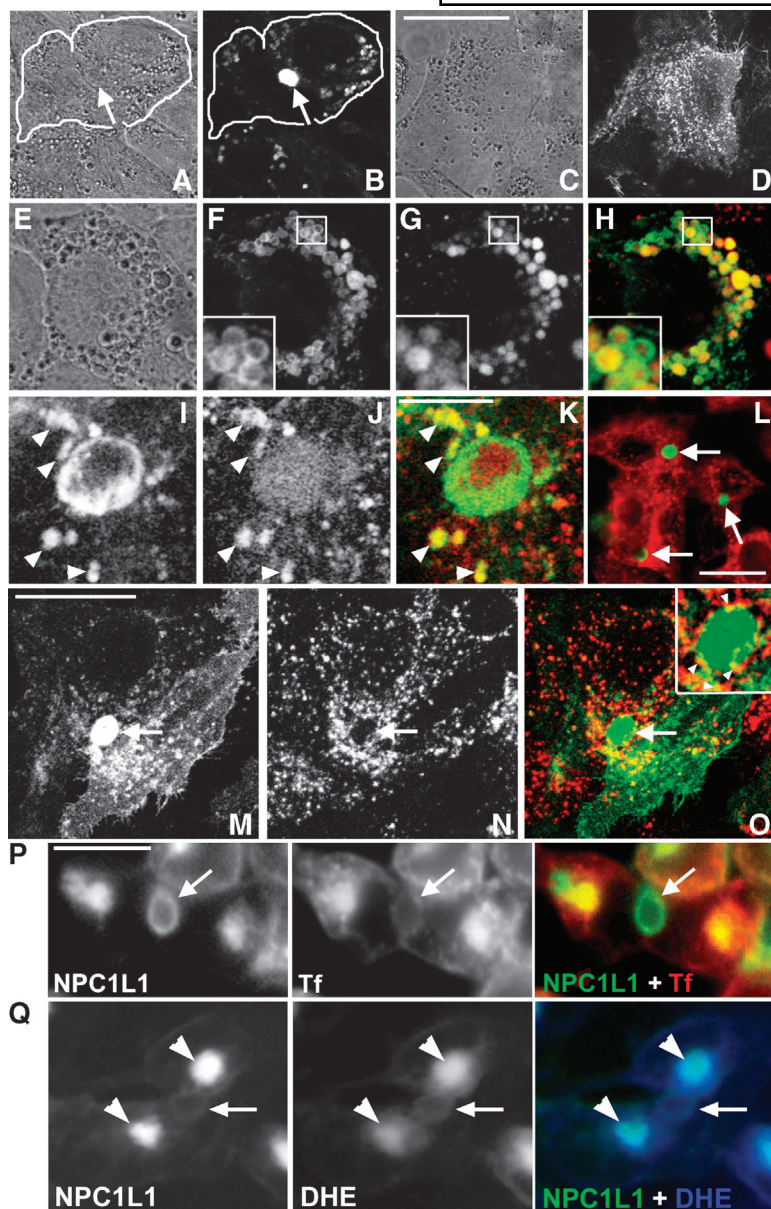
Fig. 8. Intracellular localization of NPC1L1-EGFP in polarized hepatoma cells. A, B: Polarized HepG2 cells showed high expression of NPC1L1-EGFP in the apical bile canaliculi (BC) (arrow). C, D: Nonpolarized HepG2 cells had a higher fraction of NPC1L1-EGFP in the plasma membrane than McA cells shown in Fig. 1. E–K: HepG2 cells expressing NPC1L1-EGFP were incubated with rhodamine-labeled dextran (Rh-dextran) for 1 h at 37°C, washed, and imaged on a confocal microscope. Rh-dextran stains late endosomes and lysosomes as well as the lumen of BC (30). Arrowheads indicate late endosomes and lysosomes labeled by Rh-dextran and NPC1L1-EGFP. L–P: HepG2 cells expressing NPC1L1-EGFP were incubated with 20 μg/ml Alexa546-Tf for 15 min at 37°C, washed, and chased for 30 min. B, D, F, I, M: NPC1L1-EGFP. G, J: Rh-dextran. H, K: Color overlay showing NPC1L1-EGFP in green and Rh-dextran in red. L, O: Color overlay showing NPC1L1-EGFP in green and Alexa546-Tf in red. Colocalization appears yellow to orange. Inset of O: Zoom of the BC region of the cells shown in M–O. Arrowheads point to vesicles close to the BC containing NPC1L1-EGFP as well as Alexa546-Tf. All images are confocal images except L, P, Q (wide-field images). Arrows in L point to apical BC. P: Polarized McA cells expressing NPC1L1-EGFP were incubated with Alexa546-Tf as described above, chased for 30 min, and imaged on a wide-field microscope. NPC1L1-EGFP was enriched in the apical canalicular membrane, forming a BC vacuole (arrow), and in Tf-positive vesicles resembling the subapical recycling compartment. Q: McA cells were pulse-labeled with DHE/MCD, chased for 30 min, and imaged on a wide-field microscope. NPC1L1-EGFP colocalized with DHE in the subapical recycling compartment (arrowheads) and in the canalicular membrane (arrows) in polarized McA cells. Color overlay shows DHE in blue and NPC1L1-EGFP in green. Bar, 20 μm.

membrane (Fig. 8A, B). Intracellularly, NPC1L1-EGFP could be found in Tf-containing recycling endosomes as well as in large lysososomal structures labeled with Rh-dextran in both polarized and nonpolarized HepG2 cells (Fig. 8E–O). The lysosomes contained NPC1L1-EGFP exclusively in their limiting membrane, whereas Rh-dextran was found in the lumen (Fig. 8F–H). Rh-dextran-labeled late endosomes and lysosomes containing NPC1L1-EGFP were also found in the subapical region (arrowheads in Fig. 8I–K). The central BC contained NPC1L1 in the canalicular membrane, whereas Rh-dextran was found in the lumen of the apical BC vacuole. Double-labeled vesicles having Tf as well as NPC1L1-EGFP were found in close proximity to the BC, probably resembling part of the subapical recycling compartment in those cells (Fig. 8M–O, and inset of Fig. 8O) (24, 32).

Occasionally, we found polarized McA cells, i.e., a cell couplet forming an apical BC-like vacuole (4). In those

cells, NPC1L1-EGFP became highly enriched in the apical canalicular membrane and was additionally targeted to the Tf-containing subapical recycling compartment, where NPC1L1 also colocalized with the fluorescent sterol DHE (Fig. 8P; arrowheads, Fig. 8Q). Fluorescent sterol and NPC1L1 protein resided in the canalicular membrane of polarized McA cells and HepG2 cells (arrows, Fig. 8Q and supplementary data). In polarized HepG2 cells, NPC1L1-EGFP and DHE additionally colocalized in the large scattered endosomes after prolonged chase in medium 1 (see supplementary data). Together, the results demonstrate that upon polarization of both hepatoma cell types, McA and HepG2, NPC1L1 becomes selectively targeted to the apical but not to the basolateral membrane. In contrast to McA cells, the intracellular trafficking intineraries of NPC1L1-EGFP in HepG2 cells are more heterogeneous, with recycling endosomes, late endosomes, and lysosomes, as well as kinetically defined sorting endo-

somes (not shown), as NPC1L1-positive organelles. The intracellular distribution of fluorescent sterols mimics that of NPC1L1-EGFP in polarized hepatoma cells, with the subapical recycling compartment as a sterol-rich organelle in polarized McA cells (30, 44).

NPC1L1 is highly mobile in the canalicular membrane of polarized HepG2 cells

To get insight into the distribution and dynamics of NPC1L1-EGFP in the canalicular membrane, we acquired high-resolution 3D stacks on a confocal laser scanning microscope. This method revealed that NPC1L1-EGFP localized to plane and folded microvilli-rich regions of the canalicular membrane, the latter protruding into the BC lumen of HepG2 cells (**Fig. 9A, B**). To assess protein dynamics, we performed a FRAP experiment, where fluorescence of NPC1L1-EGFP was selectively bleached in a rectangular stripe over an elliptical BC (Fig. 9C, D). Note that fluorescence of NPC1L1-EGFP recovered very rapidly, with a half-time of about 30 s (Fig. 9C–E). The same BC was bleached at the opposite site in the same manner, giving essentially the same result (Fig. 9D). This rules out a dependence of fluorescence recovery on the location of the bleach stripe relative to the canalicular membrane. This type of experiment was performed on seven different BCs, and the measured normalized mean intensity of fluorescence recovery is shown in Fig. 9E. Recovery was about 80%, suggesting that protein mobility is slightly restricted in the canalicular membrane. We found in independent spot photobleaching experiments, where just a small region of the canalicular membrane instead of the large stripe was bleached, that fluorescence recovery was indeed complete (not shown).

DISCUSSION

NPC1L1 has been identified as a sterol transporter in the intestine, but recent data support an additional function of this protein in regulating biliary cholesterol secretion from hepatocytes (1, 5, 10). We performed a detailed kinetic fluorescence imaging study to characterize the dynamics of NPC1L1 in hepatoma cells and to determine in parallel the role of this protein in sterol trafficking. Our results demonstrate that the majority of intracellular NPC1L1 colocalizes with fluorescent Tf and sterol in the ERC in nonpolarized McA cells. We provide evidence for dynamic shuttling of NPC1L1 between the plasma membrane and the ERC via peripheral sorting endosomes. Our kinetic data suggest that internalization of NPC1L1-EGFP from the plasma membrane is much slower than that of Alexa546-Tf, whereas trafficking of NPC1L1 from sorting endosomes to the ERC is fast (see Figs. 1–4). This process might contribute to keeping the fraction of NPC1L1 low in the peripheral sorting endosomes at steady state, as we found in our experiments (see Figs. 1, 3). The large amount of the protein in the ERC at steady state (about 42% of total) indicates that recycling of NPC1L1-EGFP is also a relatively slow process. Thus, overall we
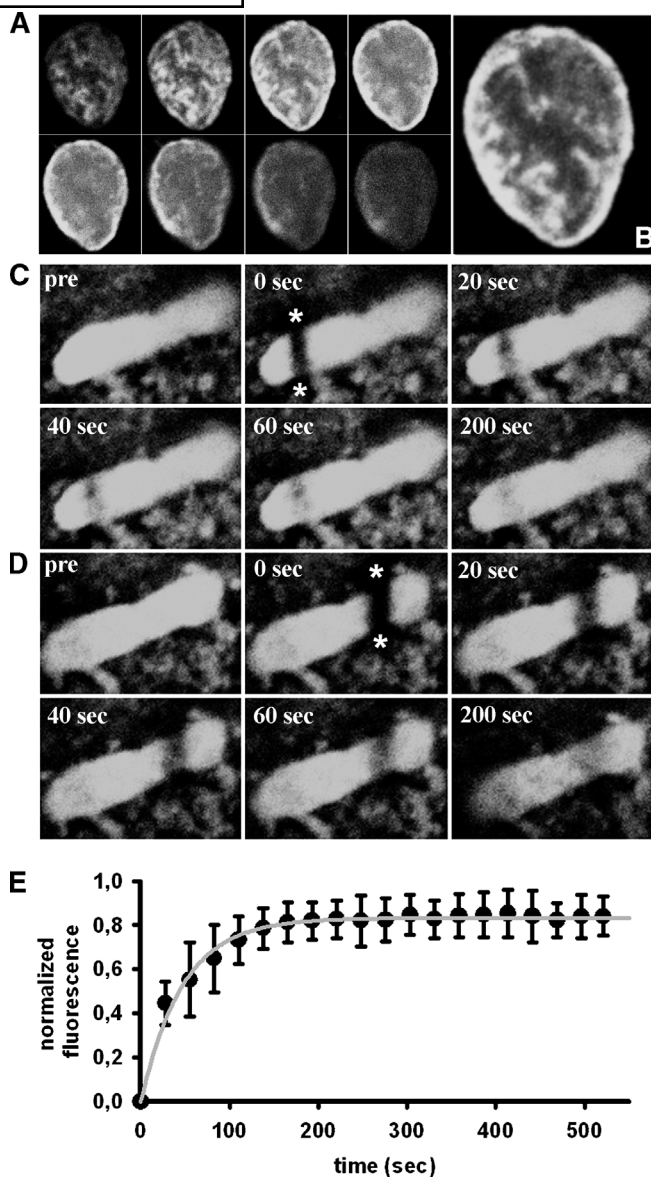

Fig. 9. Distribution and dynamics of NPC1L1 in the canalicular membrane of HepG2 cells. A, B: Polarized HepG2 cells expressing NPC1L1-EGFP were imaged on a confocal microscope in z-stacking modus with 0.5 μm step size, a pinhole diameter of one Airy disk, and an argon laser as excitation source. A: Individual planes. B: Maximum intensity projection of a BC reveals intense staining of fluorescent NPC1L1 in microvilli of the canalicular membrane protruding into the BC lumen. C, D: FRAP experiments of an elliptically shaped BC. A stripe covering the short distance over a BC, indicated by stars, was selectively bleached, and fluorescence recovery was monitored with reduced laser power for a total of 450 s. NPC1L1-EGFP diffused rapidly into the bleach stripe, irrespective of the location of this stripe. D: Repetition of experiment shown in C at the other side of the same BC. E: Quantification of fluorescence recovery from independent experiments at different BCs (mean ± SE, n = 7). Symbols, data normalized as described in Experimental Procedures. Gray line, fit to single exponential function of the form f = A*(1-exp(−k*t)) giving a half-time of fluorescence recovery of 32.5 ± 5 s.

can conclude that NPC1L1-EGFP and Alexa546-Tf share the same trafficking itineraries in McA cells but their relative abundance in various endosome populations is different due to different inter-compartment transport kinetics.

Slow internalization of NPC1L1-EGFP can probably be explained by the absence of appropriate signal motifs in NPC1L1, such as the tyrosine-based sorting motif NPXY found in the Tf receptor that is necessary for efficient collection of the Tf receptor in clathrin-coated pits (45, 46). The NPC1L1 protein also lacks the dileucine motif that is found in multispanning transmembrane proteins targeted to late endosomes or lysosomes, like NPC1, or in proteins transported to stimulus-responsive storage vesicles like GLUT4 or aquaporin 4 (45, 46). Conversely, NPC1L1 has a YQRL motif, which has been shown to target proteins like TGN38 from the plasma membrane to the Golgi apparatus (45, 46). Previous experiments, however, have shown that NPC1L1-EGFP does not colocalize with TGN38 or other Golgi markers (4). This is supported by our observation that NPC1L1 continued to colocalize with fluorescent Tf in the ERC in McA cells incubated with the microtubule-disrupting drug nocodazole (see Fig. 4), a treatment that triggers scattering of the Golgi in many cell types (20). Thus, it is unlikely that YQRL functions as a Golgi-targeting motif in NPC1L1 (45).

Our results show that acute cholesterol depletion by MCD blocks endocytosis of NPC1L1, as verified by finding a similar redistribution from the ERC to the cell surface upon MCD treatment of Alexa546-Tf (see Fig. 5). Fluorescent Tf is a marker for clathrin-dependent endocytosis, which is strictly cholesterol dependent (26, 27). Thus, it is likely that NPC1L1 is internalized by this endocytic pathway, albeit more slowly than is Tf (see Figs. 1–4). Cholesterol depletion seems to stimulate additionally recycling of NPC1L1 in nonpolarized McA cells. This was indicated by a more pronounced relocation of NPC1L1-EGFP compared with Alexa546-Tf from the ERC to the plasma membrane upon MCD treatment (see Fig. 5G). Cholesterol depletion has been shown previously to accelerate specifically recycling of the GPI-anchored folate receptor in CHO cells, whereas recycling of fluorescent Tf or sphingolipids was unaffected (47). It is also possible that the stimulated recycling of NPC1L1 upon cholesterol depletion requires a signaling mechanism inherent to the protein, e.g., the sterol-sensing domain (SSD) of NPC1L1 (45). The SSD of NPC1L1 could also regulate the intracellular targeting of the protein between the plasma membrane and the ERC. Both hypotheses are supported by our preliminary experiments, in which we generated a point mutation in the SSD of NPC1L1 (i.e., Pro703Ser). This conserved proline is also found in the NPC1 protein, where a mutation, Pro692Ser, in the SSD induced a loss-of-function phenotype with reduced delivery of LDL-derived cholesterol from LE/LYS to the endoplasmic reticulum or plasma membrane (48). We observed that mutant NPC1L1-EGFP continued to be targeted to the ERC in McA cells. However, the amount of the mutant protein, as well as of fluorescent sterol in the ERC, was significantly reduced compared with wild-type McA cells

expressing NPC1L1-EGFP, with a higher fraction of protein and sterol in the plasma membrane in mutant cells (unpublished observations). Further studies are required to uncover the molecular details of NPC1L1 transport between the ERC and the cell surface.

We show in this study that expression of NPC1L1-EGFP facilitates transport of the fluorescent sterol DHE from the plasma membrane to the ERC in McA cells (see Fig. 6). The ERC has been previously described as a sterol storage organelle that receives plasma membrane sterols by vesicular and ATP-independent nonvesicular trafficking modes (30, 35). The slow kinetics of NPC1L1-facilitated sterol accumulation in the ERC is in accordance not with rapid nonvesicular but with much slower vesicular transport of DHE to the ERC (see Fig. 7). We speculate that vesicular NPC1L1-mediated sterol transport to the ERC could contribute to NPC1L1-mediated sterol uptake from the plasma membrane in hepatocytes and perhaps also in intestinal enterocytes. This is supported by our preliminary observations using a mutant NPC1L1 with a point mutation in the SSD (see above). Cholesterol reloading using MCD-cholesterol complexes might trigger endocytosis of NPC1L1 together with sterol, thereby increasing the cellular sterol uptake. Note that the previously measured time course of NPC1L1-stimulated cholesterol uptake from MCD-cholesterol complexes in cholesterol-depleted McA cells is well in accordance with slow endocytosis of the NPC1L1 protein and with slow NPC1L1-mediated sterol targeting to the ERC (4, 25).

Activation of insulin-signaling pathways raised the cell surface fraction of NPC1L1, paralleled by a slight but significant redistribution of fluorescent sterols (see Fig. 7). Importantly, we found only in insulin-treated cells vesicles containing DHE and NPC1L1 in close proximity to the cell surface, suggesting that vesicular trafficking of both sterol and NPC1L1 is at least partially insulin regulated. Insulin-stimulated recycling from the ERC has been demonstrated previously for other proteins, e.g., for the glucose transporter GLUT4 and for fluorescent Tf, indicating that insulin signaling controls ERC-to-plasma membrane transport in general (42). Because the ERC is a sterol-rich compartment, this probably explains why we also see a stimulation of sterol transport from the ERC upon insulin treatment. In fact, insulin treatment stimulated recycling of Tf by 20%, which is about the same extent we find here for DHE [see Fig. 6 and (42)]. Because the observed effect is small, further studies in different systems are required to determine whether it is of physiological relevance for intracellular cholesterol transport.

Our observation that expression of NPC1L1-EGFP results in increased accumulation of sterol in the ERC of McA cells is supported by additional experiments performed in polarized McA cells (see Fig. 8Q). Here, DHE became highly enriched in the cholesterol-rich subapical recycling compartment, which resembles the Tf-positive ERC of nonpolarized cells (21, 22). The subapical (recycling) compartment functions as a sorting station for sphingolipids and proteins between the apical and basolateral membrane (21, 49), is required for establishment

of epithelial polarity in hepatic cells (50), and is an intra-cellular itinerary of sterol and HDL (30, 32). This endo-somal compartment was also shown to harbor intracellular ABCA1 transporter in polarized hepatic WIF-B cells, sup-porting that this organelle plays a fundamental role in hepatocellular cholesterol homeostasis (51). In HepG2 cells, NPC1L1-EGFP had a more heterogeneous distribu-tion than in McA cells, with NPC1L1 found in Tf-positive vesicles and additionally in enlarged lysosomes containing Rh-dextran (see Fig. 8). Importantly, in these cells, but not in control HepG2 cells, we found colocalization of DHE with NPC1L1-EGFP in similarly enlarged endosomes scat-tered throughout the cytoplasm (see supplementary data). We conclude that the intracellular distribution of fluo-rescent sterol mirrors that of NPC1L1-EGFP, supporting a function of this protein in intracellular sterol trafficking from the cell surface. The strong apical localization of NPC1L1, as well as the fact that fluorescent sterol and NPC1L1-EGFP colocalized in subapical vesicles, suggests a function of the protein in sterol reabsorption from the bile fluid, probably by shuttling sterol in vesicles to the subapi-cal recycling compartment and other endosomes (5).

REFERENCES

1. Altmann, S. W., H. R. J. Davis, L. J. Zhu, X. Yao, L. M. Hoos, G. Tetzloff, S. P. Iyer, M. Maguire, A. Golovko, M. Zeng, et al. 2004. Niemann-Pick C1-Like 1 protein is critical for intestinal cholesterol absorption. *Science.* **303:** 1201–1204.

2. Garcia-Calvo, M., J. Lisnock, H. G. Bull, B. E. Hawes, D. A. Burnett, M. P. Braun, J. H. Crona, H. R. J. Davis, D. C. Dean, P. A. Detmers, et al. 2005. The target of ezetimibe is Niemann-Pick C1-Like 1 (NPC1L1). *Proc. Natl. Acad. Sci. USA.* **102:** 8132–8137.

3. Davis, H. R., and E. P. Veltri. 2007. Zetia: inhibition of Niemann-Pick C1 Like 1 (NPC1L1) to reduce intestinal cholesterol absorption and treat hyperlipidemia. *J. Atheroscler. Thromb.* **14:** 99–108.

4. Yu, L., S. Bharadwaj, J. M. Brown, Y. Ma, W. Du, M. A. Davis, P. Michaely, P. Liu, M. C. Willingham, and L. L. Rudel. 2006. Cholesterol-regulated translocation of NPC1L1 to the cell surface facilitates free cholesterol uptake. *J. Biol. Chem.* **281:** 6616–6624.

5. Temel, R. E., W. Tang, Y. Ma, L. L. Rudel, M. C. Willingham, Y. A. Ioannou, J. P. Davies, L. M. Nilsson, and L. Yu. 2007. Hepatic Niemann-Pick C1-like 1 regulates biliary cholesterol concentration and is a target of ezetimibe. *J. Clin. Invest.* **117:** 1968–1978.

6. Labonte, E. D., P. N. Howles, N. A. Granholm, J. C. Rojas, J. P. Davies, Y. A. Ioannou, and D. Y. Hui. 2007. Class B type I scavenger receptor is responsible for the high affinity cholesterol binding ac-tivity of intestinal brush border membrane vesicles. *Biochim. Biophys. Acta.* **1771:** 1132–1139.

7. Sane, A. T., D. Sinnett, E. Delvin, M. Bendayan, V. Marcil, D. Menard, J. F. Beaulieu, and E. Levy. 2006. Localization and role of NPC1L1 in cholesterol absorption in human intestine. *J. Lipid Res.* **47:** 2112–2120.

8. Knöpfel, M., J. P. Davies, P. T. Duong, L. Kværnø, E. M. Carreira, M. C. Phillips, Y. A. Ioannou, and H. Hauser. 2007. Multiple plasma membrane receptors but not NPC1L1 mediate high-affinity, ezetimibe-sensitive cholesterol uptake into the intestinal brush border mem-brane. *Biochim. Biophys. Acta.* **1771:** 1140–1147.

9. Yamanashi, Y., T. Takada, and H. Suzuki. 2007. Niemann-Pick C1-like 1 overexpression facilitates ezetimibe-sensitive cholesterol and beta-sitosterol uptake in CaCo-2 cells. *J. Pharmacol. Exp. Ther.* **320:** 559–564.

10. Davis, H. R., Jr., L. J. Zhu, L. M. Hoos, G. Tetzloff, M. Maguire, J. Liu, X. Yao, S. P. Iyer, M. H. Lam, E. G. Lund, et al. 2004. Niemann-Pick C1 Like 1 (NPC1L1) is the intestinal phytosterol and choles-terol transporter and a key modulator of whole-body cholesterol homeostasis. *J. Biol. Chem.* **279:** 33586–33592.

11. Davies, J. P., and Y. A. Ioannou. 2006. The role of the Niemann-Pick C1-like 1 protein in the subcellular transport of multiple lipids and their homeostasis. *Curr. Opin. Lipidol.* **17:** 221–226.

12. Davies, J. P., C. Scott, K. Oishi, A. Liapis, and Y. A. Ioannou. 2005. Inactivation of NPC1L1 causes multiple lipid transport defects and protects against diet-induced hypercholesterolemia. *J. Biol. Chem.* **280:** 12710–12720.

13. Dunn, K. W., T. E. McGraw, and F. R. Maxfield. 1989. Iterative frac-tionation of recycling receptors from lysosomally destined ligands in an early sorting endosome. *J. Cell Biol.* **109:** 3303–3314.

14. Salzmann, N. H., and F. R. Maxfield. 1989. Fusion accessibility of endocytic compartments along the recycling and lysosomal endo-cytic pathways in intact cells. *J. Cell Biol.* **109:** 2097–2104.

15. Mukherjee, S., R. N. Ghosh, and F. R. Maxfield. 1997. Endocytosis. *Physiol. Rev.* **77:** 759–803.

16. Ghosh, R. N., and F. R. Maxfield. 1995. Evidence for nonvectorial, retrograde transferrin trafficking in the early endosomes of HEp2 cells. *J. Cell Biol.* **128:** 549–561.

17. Mayor, S., J. F. Presley, and F. R. Maxfield. 1993. Sorting of mem-brane components from endosomes and subsequent recycling to the cell surface occurs by a bulk flow process. *J. Cell Biol.* **121:** 1257–1269.

18. Jin, M., and M. D. Snider. 1993. Role of microtubules in transferrin receptor transport from the cell surface to endosomes and the Golgi complex. *J. Biol. Chem.* **268:** 18390–18397.

19. Sakai, T., S. Yamashina, and S. Ohnishi. 1991. Microtubule-disrupting drugs blocked delivery of endocytosed transferrin to the cytocenter, but did not affect return of transferrin to plasma membrane. *J. Biochem.* **109:** 528–533.

20. Baravalle, G., D. Schober, M. Huber, N. Bayer, R. F. Murphy, and R. Fuchs. 2005. Transferrin recycling and dextran transport to lyso-somes is differentially affected by bafilomycin, nocodazole, and low temperature. *Cell Tissue Res.* **320:** 99–113.

21. van Ijzendoorn, S. C., Hoekstra D. 1998. (Glyco)sphingolipids are sorted in sub-apical compartments in HepG2 cells: a role for non-Golgi-related intracellular sites in the polarized distribution of (glyco)sphingolipids. *J. Cell Biol.* **142:** 683–696.

22. Wüstner, D., S. Mukherjee, F. R. Maxfield, P. Müller, and A. Hermann. 2001. Vesicular and nonvesicular transport of phosphatidylcholine in polarized HepG2 cells. *Traffic.* **2:** 277–296.

23. Sheff, D. R., E. A. Daro, M. Hull, and I. Mellman. 1999. The receptor recycling pathway contains two distinct populations of early endosomes with different sorting functions. *J. Cell Biol.* **145:** 123–139.

24. Wüstner, D. 2006. Quantification of polarized trafficking of transfer-rin and comparison with bulk membrane transport in hepatic cells. *Biochem. J.* **400:** 267–280.

25. Brown, J. M., L. L. Rudel, and L. Yu. 2007. NPC1L1 (Niemann-Pick C1-like 1) mediates sterol-specific unidirectional transport of non-esterified cholesterol in McArdle-RH7777 hepatoma cells. *Biochem. J.* **406:** 273–283.

26. Subtil, A., I. Gaidarov, K. Kobylarz, M. A. Lampson, J. H. Keen, and T. E. McGraw. 1999. Acute cholesterol depletion inhibits clathrin-coated pit budding. *Proc. Natl. Acad. Sci. USA.* **96:** 6775–6780.

27. Rodal, S. K., G. Skretting, O. Garred, F. Vilhardt, B. van Deurs, and K. Sandvig. 1999. Extraction of cholesterol with methyl-beta-cyclodextrin perturbs formation of clathrin-coated endocytic vesi-cles. *Mol. Biol. Cell.* **10:** 961–974.

28. Sormunen, R., S. Eskelinen, and V. P. Lehto. 1993. Bile canaliculus formation in cultured HEPG2 cells. *Lab. Invest.* **68:** 652–662.

29. van IJzendoorn, S. C., M. M. Zegers, J. W. Kok, and D. Hoekstra. 1997. Segregation of glucosylceramide and sphingomyelin occurs in the apical to basolateral transcytotic route in HepG2 cells. *J. Cell Biol.* **137:** 347–357.

30. Wüstner, D., A. Herrmann, M. Hao, and F. R. Maxfield. 2002. Rapid nonvesicular transport of sterol between the plasma membrane domains of polarized hepatic cells. *J. Biol. Chem.* **277:** 30325–30336.

31. Tannert, A., D. Wüstner, J. Bechstein, P. Müller, P. F. Devaux, and A. Herrmann. 2003. Aminophospholipids have no access to the lumi-nal side of the biliary canaliculus: implications for the specific lipid composition of the bile fluid. *J. Biol. Chem.* **278:** 40631–40639.

32. Wüstner, D., M. Mondal, A. Huang, and F. R. Maxfield. 2004. Differ-ent transport routes for high density lipoprotein and its associated free sterol in polarized hepatic cells. *J. Lipid Res.* **45:** 427–437.

33. van IJzendoorn, S. C., and D. Hoekstra. 1999. Polarized sphingo-lipid transport from the subapical compartment: evidence for dis-tinct sphingolipid domains. *Mol. Biol. Cell.* **10:** 3449–3461.

34. Wüstner, D. 2005. Improved visualization and quantitative analysis of fluorescent membrane sterol in polarized hepatic cells. *J. Microsc.* **220:** 47–64.

35. Hao, M., S. X. Lin, O. J. Karylowski, D. Wüstner, T. E. McGraw, and F. R. Maxfield. 2002. Vesicular and non-vesicular sterol transport in living cells. The endocytic recycling compartment is a major sterol storage organelle. *J. Biol. Chem.* **277:** 609–617.

36. Wüstner, D., M. Mondal, I. Tabas, and F. R. Maxfield. 2005. Direct observation of rapid internalization and intracellular transport of sterol by macrophage foam cells. *Traffic.* **6:** 396–412.

37. Yamashiro, D. J., B. Tycko, S. R. Fluss, and F. R. Maxfield. 1984. Segregation of transferrin to a mildly acidic (pH 6.5) para-Golgi compartment in the recycling pathway. *Cell.* **37:** 789–800.

38. Wüstner, D. 2005. Mathematical analysis of hepatic high density lipoprotein transport based on quantitative imaging data. *J. Biol. Chem.* **280:** 6766–6779.

39. Mukherjee, S., T. T. Soe, and F. R. Maxfield. 1999. Endocytic sorting of lipid analogues differing solely in the chemistry of their hydrophobic tails. *J. Cell Biol.* **144:** 1271–1284.

40. Wüstner, D. 2007. Plasma membrane sterol distribution resembles the surface topography of living cells. *Mol. Biol. Cell.* **18:** 211–228.

41. Dahm, T., J. White, S. Grill, J. Füllekrug, and E. H. K. Stelzer. 2001. Quantitative ER ←→ Golgi transport kinetics and protein separation upon Golgi exit revealed by vesicular integral membrane protein 36 dynamics in live cells. *Mol. Biol. Cell.* **12:** 1481–1498.

42. Maxfield, F. R., and T. E. McGraw. 2004. Endocytic recycling. *Nat. Rev. Mol. Cell Biol.* **5:** 121–132.

43. Pipalia, N. H., M. Hao, S. Mukherjee, and F. R. Maxfield. 2006. Sterol, protein and lipid trafficking in Chinese hamster ovary cells with Niemann-Pick type C1 defect. *Traffic.* **8:** 130–141.

44. Gagescu, R., N. Demaurex, R. G. Parton, W. Hunziker, L. A. Huber, and J. Gruenberg. 2000. The recycling endosome of Madin-Darby canine kidney cells is a mildly acidic compartment rich in raft components. *Mol. Biol. Cell.* **11:** 2775–2791.

45. Davies, J. P., B. Levy, and Y. A. Ioannou. 2000. Evidence for a Niemann-Pick C (NPC) gene family: identification and characterization of NPC1L1. *Genomics.* **65:** 137–145.

46. Bonifacino, J. S., and L. M. Traub. 2003. Signals for sorting of transmembrane proteins to endosomes and lysosomes. *Annu. Rev. Biochem.* **72:** 395–447.

47. Mayor, S., S. Sabharanjak, and F. R. Maxfield. 1998. Cholesterol-dependent retention of GPI-anchored proteins in endosomes. *EMBO J.* **17:** 4626–4638.

48. Millard, E. E., S. E. Gale, N. Dudley, J. Zhang, J. E. Schaffer, and D. S. Ory. 2005. The sterol-sensing domain of the Niemann-Pick C1 (NPC1) protein regulates trafficking of low density lipoprotein cholesterol. *J. Biol. Chem.* **280:** 28581–28590.

49. van IJzendoorn, S. C., and Hoekstra, D. 2000. Polarized sphingolipid transport from the subapical compartment changes during cell polarity development. *Mol. Biol. Cell.* **11:** 1093–1101.

50. Hoekstra, D., D. Tyteca, and S. C. van IJzendoorn. 2004. The subapical compartment: a traffic center in membrane polarity development. *J. Cell Sci.* **117:** 2183–2192.

51. Neufeld, E. B., S. J. Demosky, Jr., J. A. Stonik, C. Combs, A. T. Remaley, N. Duverger, S. Santamarina-Fojo, and H. B. Brewer, Jr. 2002. The ABCA1 transporter functions on the basolateral surface of hepatocytes. *Biochem. Biophys. Res. Commun.* **297:** 974–979.